

Prospects for Improved Magnesocene-Based Magnesium Battery Electrolytes

Piotr Jankowski,^[a, b, c, d] Rainer Schwarz,^[e] Anna Randon-Vitanova,^[f] Reza Younesi,^[c, g] Mario Wachtler,^{*[e, g]} and Patrik Johansson^{*[a, c]}

Magnesium batteries are currently attracting a lot of interest as a next generation battery technology. One critical issue is to find a suitable electrolyte and herein we explore an electrolyte based on magnesocene (MgCp_2) in tetrahydrofuran (THF), aiming for low-voltage Mg batteries, with respect to: Mg plating characteristics, electrochemical stability windows, electrolyte speciation, and electrolyte decomposition reactions; both experimentally and computationally. Overall, the electrolyte does not seem to decompose on a Mg metal anode and most likely reduced solvation of Mg^{2+} by the Cp^- anion is important

and species such as $\text{MgCp}_2\text{THF}_2$ may play an important role for Mg plating with small overpotential. The oxidation limit is largely determined by the Cp^- anion and density functional theory predicted oxidation reactions point to polymerized end-products to be possible. Furthermore, *in silico* substitution studies enable us to establish the prospects of some Cp^- anion derivatives to further improve the oxidative stability, but still the Mg^{2+} solvation must be monitored for ease of reduction and Mg plating.

1. Introduction

The dual intercalation chemistry, *i.e.* the rocking-chair concept, behind the today omnipresent lithium-ion batteries (LIBs) was developed in the 1970's and enabled the commercialization of LIBs *ca.* 20 years later.^[1] Numerous large improvements along the way have been made and these are continued-not the least

in terms of production and cost. With the maturity reached for LIBs, fundamental research on rechargeable next generation batteries (NGBs) has turned to enable the use of metal anodes; lithium metal as well as several multivalent battery chemistries have been in focus: Mg, Ca, Al, *etc.*^[2] Much of this has remained merely an academic curiosity with rather few research groups active, even if the landscape is changing fast. In contrast a significant amount of research has been devoted to Mg metal anode based batteries, especially after that proof-of-concept was shown by Aurbach in 2000.^[3] While the standard potential of Mg metal is ~ 670 mV higher than that of Li metal, only half the number of ions are necessary for an equivalent charge transfer. Furthermore, the naked ionic radius of Mg^{2+} (0.72 Å) is very close to that of Li^+ (0.76 Å)^[4] why there is promise for finding suitable cathodes to host Mg^{2+} by intercalation. We can also fundamentally expect a Mg metal anode based battery to be both more sustainable and less costly *vs.* a Li metal anode based, all other things considered equal, looking at the abundances in the Earth's crust, *ca.* 27640 *vs.* 18 ppm^[5] and the raw material cost, *ca.* 4740 *vs.* 20745 \$/ton equivalent,^[6] respectively.

A critical issue for Mg metal anode based batteries, indeed true for most NGBs based on metal anodes but even more so for Mg, is to find a suitable electrolyte; classical electrolytes based on simple salts result in a strong passivation of the Mg metal anode, which prevents reversible plating and stripping of Mg, while electrolytes capable of activating the magnesium surface by metal chloride complexes or chlorine-containing metal-organic compounds, causes notable corrosion problems at the cell level.^[7-9] Additional problems arise due to difficulties to make reliable electrochemical measurements using Mg metal anodes.^[10] The upsurge in interest in Mg battery research the last 3–5 years has produced a few reports on new Mg-salts especially developed and employed in order to create Mg

[a] Dr. P. Jankowski, Prof. Dr. P. Johansson
Chalmers University of Technology
Department of Physics
41296 Göteborg, Sweden
E-mail: patrik.johansson@chalmers.se

[b] Dr. P. Jankowski
Warsaw University of Technology
Faculty of Chemistry
00-664 Warsaw, Poland

[c] Dr. P. Jankowski, Prof. Dr. R. Younesi, Prof. Dr. P. Johansson
ALISTORE-European Research Institute
CNRS FR 3104, Hub de l'Energie
Rue Baudelocque, 80039 Amiens, France

[d] Dr. P. Jankowski
Technical University of Denmark
Department of Energy Conversion and Storage
2800 Kgs. Lyngby, Denmark

[e] Dr. R. Schwarz, Dr. M. Wachtler
ZSW-Zentrum für Sonnenenergie-und
Wasserstoff-Forschung Baden-Württemberg
89081 Ulm, Germany
E-mail: mario.wachtler@nyfikna.com

[f] Dr. A. Randon-Vitanova
Honda R&D Europe (Deutschland) GmbH
63073 Offenbach, Germany

[g] Prof. Dr. R. Younesi, Dr. M. Wachtler
Uppsala University
Department of Chemistry-Ångström Laboratory
75120 Uppsala, Sweden

© 2021 The Authors. Batteries & Supercaps published by Wiley-VCH GmbH. This is an open access article under the terms of the Creative Commons Attribution Non-Commercial NoDerivs License, which permits use and distribution in any medium, provided the original work is properly cited, the use is non-commercial and no modifications or adaptations are made.

conducting electrolytes.^[11–13] These often have the dual aim of allowing for reversible plating and stripping of Mg metal and to extend the anodic electrochemical stability limit to allow for medium to high voltage cells (>3.0 V).

However, the common drawback is that these new Mg-salts rely on both large and rather complex anions, that are cumbersome to create, and not seldom also extensively use fluorination; costly in production and also problematic in the battery recycling stage, which should be seriously considered at the very on-set of embarking towards any NGB technology. With a bit of a different stance, the bis(cyclopentadienyl)-magnesium (magnesocene, MgCp₂) salt (Figure 1) was introduced by some of us as the solute for new chlorine-free electrolytes, dissolved in tetrahydrofuran (THF), aiming for low voltage (<2.0 V) Mg batteries.^[14] While this aim of course fundamentally limits the cell energy densities possible, a 2.0 V cell model employing a hypothetical cathode of 200 mAh/g still allows for ca. 190 Wh/kg and 400 Wh/l at the cell level (Figure 2)¹. Arguably this comes with improved safety and much more prospect for actually finding a suitable active material on the cathode side, but must anyhow likely target other markets than portable electronics or electric vehicles due to the low cell voltage.

Unlike its highly stable homologue ferrocene *i.e.* FeCp₂, MgCp₂ shows some dissociation in solvents with electron donor properties, such as ethers, resulting in conductive electrolytes, as first systematically studied by W. Strohmeier *et al.*^[16,17] already in 1962. For THF, as well as for other donor solvents of low permittivity, they concluded that MgCp₂ behaves as a weak 1-1-valent electrolyte [Eq. (1)]:



and thus that Mg²⁺, as would have been the result of a complete dissociation as a 2-1-valent electrolyte, is not present. In addition, as a minimum was found in the equivalent ion

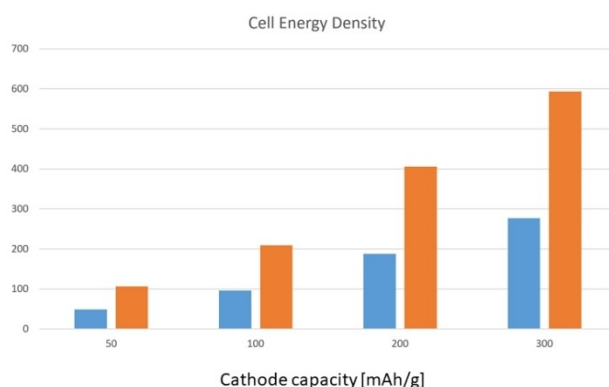


Figure 2. Modelled energy densities (blue Wh/kg, orange Wh/l) for hypothetical 2.0 V Mg battery cells.

¹ Using a rough model that anyhow comprises a thin Mg metal anode, a realistic loading and porosity of electrolyte/separator and cathode, and includes current collector and packaging material.

conductivity at high salt concentrations, they concluded that also higher aggregates were formed according to [Eqs. (2), (3)]:



Using classical electrolyte theory^[18,19] the dissociation constants K_1 and K_3 were estimated as [Eqs. (4), (5)]:

$$K_1 = [\text{MgCp}^+][\text{Cp}^-]/[\text{MgCp}_2] = 5 \times 10^{-9} \quad (4)$$

$$K_3 = [\text{MgCp}_2][\text{MgCp}^+]/[\text{Mg}_2\text{Cp}_3^+] \\ \equiv [\text{MgCp}_2][\text{Cp}^-]/[\text{MgCp}_3^-] = 1 \times 10^{-3} \quad (5)$$

A proper understanding of the origin of the dissociation and also the ion conductivity of MgCp₂ based electrolytes can be obtained starting from the MgCp₂ structure. In the gas phase and in the solvent-free solid state MgCp₂ assumes a classical sandwich structure in which both Cp rings are η⁵-coordinated, as is also known to be the case for FeCp₂.^[15,20–22] Whereas the eclipsed parallel conformation is prevailing in the gas phase,^[20] the staggered antiparallel conformation is present in the solid state.^[15,21–22] In contrast, solvent-containing crystals are obtained, when MgCp₂ is crystallised from Lewis base donor solvent solution^[22–24] and for THF as solvent MgCp₂(THF)₂ is the resulting *solid* complex wherein the two THF molecules are coordinated to the Mg-center via the O atoms. Due to space restrictions one of the Cp rings is pushed from η⁵- to η¹-coordination.^[23,25] Mg NMR spectroscopy of MgCp₂ dissolved in THF seem to indicate that MgCp₂ in *solution* is coordinated by 2 to 3 THF molecule,^[23] but to the best of our knowledge, no information is available on the structure, but can be assumed to resemble the structure of the solvated solid. This thus may explain why MgCp₂ dissociates at least partly in THF and it can also be assumed that the dissociated cation and the triplet ions are both solvated by THF.

Ultimately, the above explains why it is possible to create MgCp₂ based electrolytes with ionic conductivities in the order of 10⁻² mS/cm.^[16,17] While this is two orders of magnitude lower than the commonly accepted 1 mS/cm target set for LIB electrolytes, the more interesting observation is that high Mg plating and stripping current densities, quite comparable to other electrolytes, can be obtained for a 0.5 M MgCp₂ in THF electrolyte.^[14] This is indeed a much better key performance indicator than the ionic conductivity alone, especially for NGBs employing metal anodes. We note in passing that THF was early on employed as battery solvent due to its combination of wide liquid range, low viscosity, and overall versatility,^[25] but its electrochemical stability window (ESW), ca. 4.0 V vs. Li⁺/Li⁰ on Pt, made it of less interest than *e.g.* carbonate ethers for many (most) Li-based battery chemistries.^[26]

The aim of the present work is at the on-set basically two-fold; we want to prove experimentally that/if the magnesocene based electrolyte is stable at the Mg stripping/plating potentials and we also want to identify what species that is/are limiting the ESW. We start to address this first by investigating

the quality of the electroplated Mg by X-ray photoelectron spectroscopy (XPS) and these experimental data are further corroborated by density functional theory (DFT) calculations, which also address the stability of the electrolyte. Second, the DFT calculations are first used to in detail screen for and reveal the species present in the (bulk) electrolyte, as well as the thermodynamic and electrochemical stabilities of these species. These DFT calculations, however, also provide unique information on the reduction and oxidation reaction paths and the reaction products created at the electrode surfaces. As a final, additional and more forwarding-looking aim, we herein do different *in silico* substitutions on the Cp-rings in order to enable us to suggest some possible routes towards more stable electrolytes based on MgCp₂-derivatives.

Experimental and Computational

Electrode preparation

The Mg-on-Cu electrodes, needed for the subsequent XPS studies of the quality of the electroplated Mg, were electrochemically prepared as follows: A 3-electrode laboratory test cell (EL-Cell, ECC-Ref) was assembled with planar Cu foil (Schlenk, 99.95%, dried at 120 °C under vacuum) as working electrode, Mg foil (Gallium Source, 99.95%, polished with grain 1200 abrasive paper) as counter electrode, and Mg wire (Goodfellow, 99.9%, polished with grain 1200 abrasive paper) as reference electrode. 0.5 mol/L MgCp₂ (ABCR, 99.99%, received in ampules under Ar, used as received) in THF (Sigma Aldrich, 99.9%, inhibitor-free, dried with Na and benzophenone prior to use) and 0.5 mol/L Mg(BH₄)₂ (Sigma Aldrich, 99.5%, used as received) in THF served as the two different electrolytes. Three layers of separator were used, comprising of a central borosilicate glass fibre layer (Whatman, GF/A), to ensure an ample reservoir of electrolyte in the cell, sandwiched between two microporous polyolefin layers (Celgard, 2325, trilayer: PP-PE-PP), to prevent direct contact between the glass fibre separator and the electrodes and thereby electrode contamination by rests of glass fibres, which are known to be difficult to fully remove during disassembly and by washing. The cell was first subjected to formation by performing five cyclic voltammetry (CV) cycles between -0.5 and 1.4 V vs. Mg²⁺/Mg⁰ at a scan rate of 10 mV/s, and was then charged potentiostatically at a working electrode potential of -0.5 V vs. Mg²⁺/Mg⁰ until 10 C/cm² Mg were deposited onto the Cu foil, using a Bio-Logic VMP3 multi-channel potentiostat/galvanostat. After cycling, the electrode was extracted from the cell and washed with THF to remove electrolyte residuals. All the electrolyte preparation, cell assembly and disassembly, and electrode washing were performed in a glovebox with Ar atmosphere. A SEM image of the Mg-on-Cu electrode was recorded with a LEO 1530 VP microscope from Zeiss using an acceleration voltage of 5.0 kV and a secondary electron detector.

X-ray photo-electron spectroscopy (XPS)

The XPS measurements were performed using a Perkin Elmer PHI 5500 system with monochromatic Al K α radiation (excitation energy of 1486 keV) and an electron emission angle of 45°. All spectra were energy calibrated by using the hydrocarbon peak at a binding energy of 285.0 eV. The samples were prepared in an Ar-filled glovebox, mounted on a sample plate and transferred in an air-tight transfer-cup with no air exposure.

Density functional theory (DFT) calculations

All calculations were carried out using the Gaussian16 software package^[27] and all geometries of various hypothetical species optimized using the M06-2X DFT functional^[28] and the Pople 6-311++G(d,p) basis set. To better mimic the electrolyte surrounding the conductor-like polarizable continuum model (C-PCM)^[29] using parameters for THF was applied for all species. For these relatively small systems, *i.e.* all various hypothetical Mg_xCp_yTHF_z species and derivatives thereof, the initial starting guesses were created manually and after geometry optimization the local minima as well as the transition state geometries were both confirmed by frequency calculations. For the property evaluations, the reduction and oxidation potentials were calculated from a thermodynamic cycle, using our previously established procedure,^[30] while the charge distributions were obtained from Natural Population Analysis (NPA).^[31] All the formation energies of different species were calculated based on the electronic energies, with respect to single, uncoordinated cation, anion and solvent molecules as references (0 kJ mol⁻¹).

2. Results and Discussion

2.1. Surface Characterization of Electroplated Mg

The anodic stability of MgCp₂ in THF electrolytes was previously investigated by some of us,^[14] where by using linear sweep voltammetry the onset potentials for electrolyte oxidation were determined to 1.5–1.8 V vs. Mg²⁺/Mg⁰ dependent on the electrode used, with 1.7 V resulting for Cu. Furthermore, using CV the stripping/plating of Mg on dendritic Cu foil was found at potentials down to -0.5 V, and this together with very stable voltammograms and amounts of Mg deposited and stripped per cycle over 500 cycles. Analysis of the cycled electrolyte by FTIR and ¹³C and ¹H NMR spectroscopy revealed no new species formed.^[14]

In the present study we move into the details of the cathodic stability of the electrolyte during Mg plating conditions using XPS characterization. For this, Mg was deposited onto a planar Cu foil, applying five CV cycles for formation (Figure 3), followed by potentiostatic electrodeposition at -0.5 V vs. Mg²⁺/Mg⁰. A comparison of the formation CVs (Figure 3) reveals *ca.* five-fold higher current densities for the MgCp₂ based electrolyte as compared to the Mg(BH₄)₂ based, with very small stripping/plating overvoltage for the former, while severe for the latter. Whereas the current density increases slightly during the first few cycles for the MgCp₂ based electrolyte, which indicates electrode activation, for the Mg(BH₄)₂ based electrolytes it decreases, which could point to electrode passivation. Please note that the current densities used here are generally lower than those used within Ref. [14], the reason being the lower effective surface area of a planar Cu foil as compared to a dendritic.

The Mg 2p spectra (Figure 4) indicate that the plating made from the 0.5 M MgCp₂ in THF electrolyte consists of more or less pure Mg metal at a binding energy of *ca.* 50 eV.^[32,33] There is no major passivation film composed of electrolyte degradation products observed, and thus this agrees well with the NMR and IR spectroscopy results,^[14] but some minor contributions

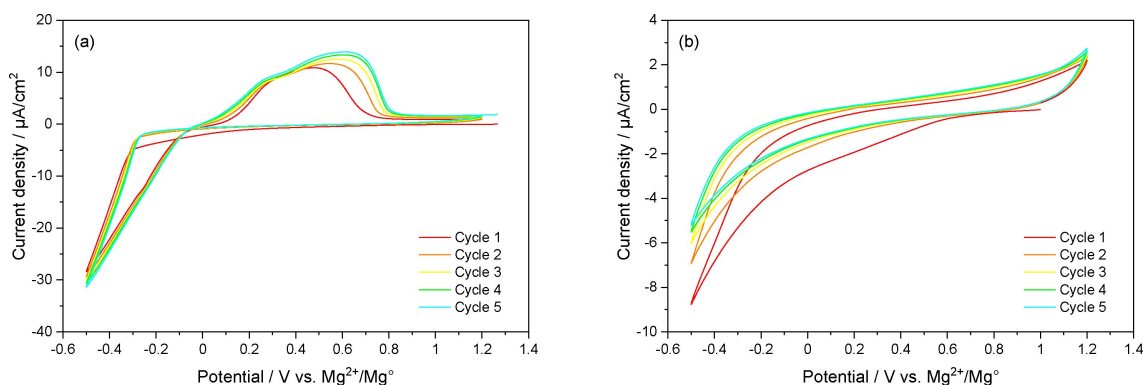


Figure 3. Initial CV cycles (at 10 mV/s) used as formation before electrodeposition of Mg on Cu from a) 0.5 M MgCp_2 in THF and b) from 0.5 M $\text{Mg}(\text{BH}_4)_2$ in THF.

Species	Coordination	E_{red} [V vs. $\text{Mg}^{2+}/\text{Mg}^0$]	E_{ox} [V vs. $\text{Mg}^{2+}/\text{Mg}^0$]	E_{int} [kJ/mol]	Structure
Cp^-	n/a	-2.38	1.86	0	6a
MgCpTHF_2^+	$\eta^5 + 2 \times \text{O}$	-0.24	4.66	-516	6b
MgCpTHF_3^+	$\eta^5 + 3 \times \text{O}$	-0.99	4.35	-616	6c
MgCpTHF_4^+	$\eta^1 + 4 \times \text{O}$	-0.98	3.87	-675	6d
MgCpTHF_5^+	$\eta^1 + 5 \times \text{O}$	-1.08	3.21	-686	6e
MgCp_2THF	$2 \times \eta^5 + \text{O}$	-1.41	3.44	-607	6f
$\text{MgCp}_2\text{THF}_2$	$\eta^5 + \eta^1 + 2 \times \text{O}$	-1.49	3.02	-667	6g
$\text{MgCp}_3\text{THF}^-$	$\eta^5 + 2 \times \eta^1 + \text{O}$	-1.90	2.10	-655	6h
$\text{Mg}_2\text{Cp}_3\text{THF}_4^+$	$2 \times [\eta^5 + \eta^1 + 2 \times \text{O}]$	-0.94	3.97	-1264 ($2x-632$)	6i

can be observed from MgO in the O 1s spectrum and from carbonate and ether species in C 1s spectrum. It is, however, difficult to conclude whether these originate from electrolyte decomposition or were formed in the sample preparation step (*i.e.* rinsing the electrodes with solvents inside the glovebox). In contrast, the Mg plated from the 0.5 M $\text{Mg}(\text{BH}_4)_2$ in THF electrolytes shows a wide and to higher energy shifted Mg 2p signal between 50–53 eV that suggests formation of different Mg species such as Mg– CH_3 species in addition to metallic Mg. Additionally, the C 1s and O 1s spectra display major contribution from ether and carboxylate species and the B 1s spectrum reveals the presence of boron in at least four different chemical environments. It is thus apparent that the 0.5 M $\text{Mg}(\text{BH}_4)_2$ in THF electrolyte is at least partly decomposed. It also shows on the sensitivity of the XPS method to reveal these events. Note that also the pristine Mg metal foil shows signals from ubiquitous C and O impurities, and thus these are not signs *per se* of electrolyte degradation, but an important observation for all further XPS analysis of Mg metal anode based batteries and points to the challenges associated with preparing “clean” Mg metal even under the controlled atmosphere in an Ar-filled glovebox. Finally, the overall appearance of a typical Mg-on-Cu electrode deposit from the 0.5 M MgCp_2 in THF electrolytes is shown in the SEM micrograph (Figure 5a). The EDX analysis of the deposit (Figure 5b) identifies Mg as the main element with some traces of C and O, which corroborates the above XPS results.

2.2. Electrolyte Speciation and Reactions

To better understand the electrolyte system, the species formed were explored using DFT calculations. The dissolution of MgCp_2 in THF results in solvation, dissociation and formation of different species, with more or less complicated structure, and we therefore sample the chemical space of primarily the first solvation shell of Mg^{2+} , for the system $\text{Mg}_x\text{Cp}_y\text{THF}_z$ (Figure 6 and Table 1). The structure of the pure salt, MgCp_2 , is experimentally well-known and the calculations easily reproduce it, resulting in coordination by the η^5 ring electron density from both Cp-rings. The interaction energy (-558 kJ mol^{-1}) naturally decreases as function of additional interactions with THF solvent molecules. A maximum of two THF per Mg^{2+} can be accommodated and the addition of the second THF changes the Mg–Cp coordination for one of the Cp^- anions from being η^5 to η^1 , in accordance with experimental data.^[23] This is also reflected in the NPA: for MgCp_2 and MgCp_2THF the charge distribution is uniform, $-0.41 |e|$ per carbon atom, but in $\text{MgCp}_2\text{THF}_2$ (-667 kJ mol^{-1}) one Cp entity displays a shifted electron density towards the coordinating carbon atom ($-0.55 |e|$).

Introduction of a third THF solvent molecule was attempted, but rendered only increased energy and no stable structure. The most interesting possibility is then rather to dissociate one anion from $\text{MgCp}_2\text{THF}_2$ to form a MgCpTHF_2^+ cation, but this is not thermodynamically preferred (-516 kJ mol^{-1}). However, it can be supported by more solvent molecules present as a step-wise introduction of THF solvent

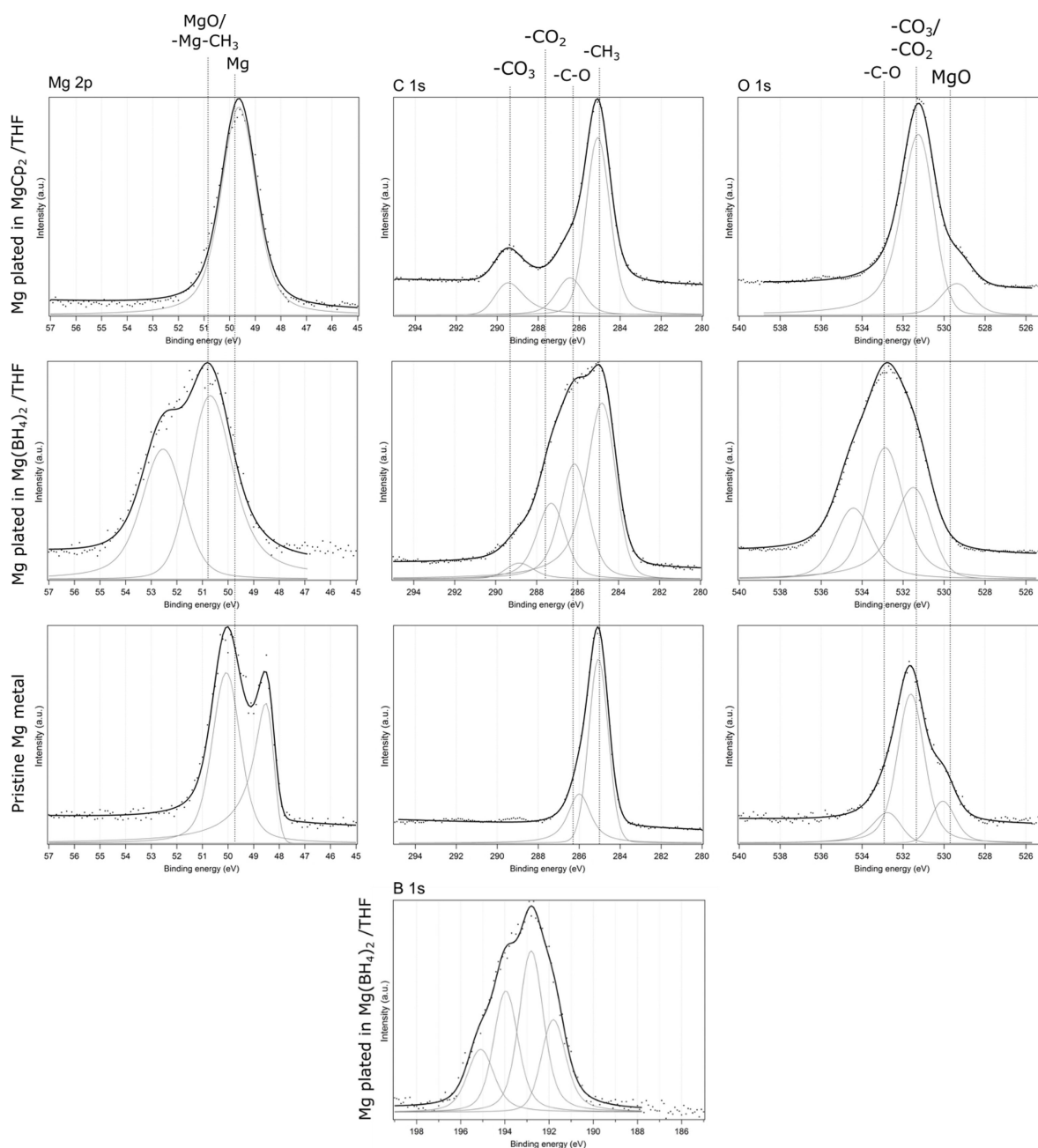


Figure 4. XPS spectra for a pristine Mg metal foil as reference vs. Mg electroplated from 0.5 M MgCp_2 in THF and from 0.5 M $\text{Mg}(\text{BH}_4)_2$ in THF.

molecules reduces the energy: -677 and -686 kJ mol^{-1} for MgCpTHF_4^+ and MgCpTHF_5^+ , respectively. This indicates a thermodynamic driving force towards salt dissociation and charge carrier creation. Structurally, as above due to steric effects, the interactions for the Cp entity change to η^1 as function of number of THF solvent molecules. While this reduces the cation-anion interaction, any further dissociation is unlikely, as e.g. formation of $\text{Mg}(\text{THF})_6^{2+}$ would require an increase up to ca. -575 kJ mol^{-1} .^[34]

Higher aggregate formation was attempted by reacting MgCpTHF_5^+ with $\text{MgCp}_2\text{THF}_2$ rendering $\text{Mg}_2\text{Cp}_3\text{THF}_x$ structures with $x_{\text{max}}=4$, which can be considered “dimers” of $\text{MgCp}_2\text{THF}_2$, but with the weakly coordinated (η^1) central Cp^- anion being

shared between the two Mg cations (Table 2). Thus maximum two THF solvent molecules per Mg cation and the formation is not thermodynamically favored. The higher number of solvent molecules in the MgCpTHF_5^+ structure is a key feature for its dissociation, by the right balance between the interaction with the rather bulky anions and with several THF solvent molecules

Table 2. DFT calculated reactions and energies for $\text{MgCp}_2\text{THF}_2$.	
Dissociation reactions	ΔE [kJ/mol]
$\text{MgCp}_2\text{THF}_2 + 3 \text{ THF} \rightarrow \text{MgCpTHF}_5^+ + \text{Cp}^-$	-19
$\text{MgCp}_2\text{THF}_2 + \text{Cp}^- \rightarrow \text{MgCp}_3\text{THF}^- + \text{THF}$	12
$\text{MgCp}_2\text{THF}_2 + \text{MgCpTHF}_5^+ \rightarrow \text{Mg}_2\text{Cp}_3\text{THF}_4^+ + 3 \text{ THF}$	90

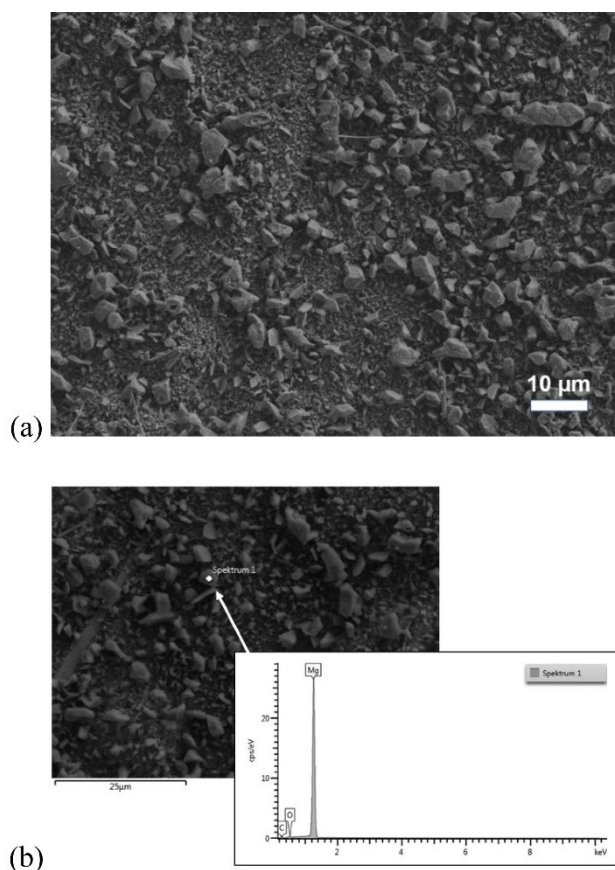


Figure 5. a) SEM micrograph and b) typical EDX spectrum of the Mg-on-Cu electrode as obtained by electrodeposition using the 0.5 M MgCp_2 in THF electrolyte.

that can occupy less space in coordination shell. At the same time, the released Cp^- could potentially be coordinated and replace THF solvent molecules in $\text{MgCp}_2\text{THF}_2$ and release a THF solvent molecule and form $\text{MgCp}_3\text{THF}^-$, but again it is connected with an increase in energy (-655 kJ mol^{-1}). Altogether, thermodynamically the dominant species are MgCpTHF_5^+ and Cp^- , but co-existing with several other species (Table 1).

Moving to the DFT analysis of the ESW of the electrolyte, which is limited by the species most vulnerable to reduction and oxidation, *i.e.* the calculated E_{red} and E_{ox} we first of all find all species to exhibit cathodic stabilities far below 0 V vs. $\text{Mg}^{2+}/\text{Mg}^0$. This is in line with our experimental observations of no

passivation film being formed on the Mg metal anode during cycling. While this stability is a huge advantage, precluding passivation film formation, the electrolyte must also enable electron transfer in order to efficiently plate magnesium. Several reactions leading to metallic magnesium were assessed and their potentials are predicted to be fairly close to 0 V vs. $\text{Mg}^{2+}/\text{Mg}^0$ (Table 3). For MgCpTHF_5^+ the extensive solvation affects the electrode process, resulting in appreciable overpotentials; by -0.18 V for a simple reaction with release of the anion and THF solvent molecules, and by -0.57 V for a more complicated reactions generating *e.g.* $\text{MgCp}_2\text{THF}_2$ or $\text{MgCp}_3\text{THF}^-$. Experimentally, however, the overpotential is always small, why rather other species may play an important role in the magnesium plating reaction mechanism. A change such as loss of a single THF ligand, from MgCpTHF_5^+ to MgCpTHF_4^+ , reduces the reaction potential to -0.05 V (*i.e.* 50 mV overpotential). Still one THF ligand less around the central Mg significantly promotes the reduction process, for MgCpTHF_3^+ it is 0.50 V vs. $\text{Mg}^{2+}/\text{Mg}^0$. Thus partial desolvation prior to the electron transfer seems very likely, but alternatively other species may also contribute. Less solvated and neutral species, such as $\text{MgCp}_2\text{THF}_2$, in fact renders a potential of 0.22 V vs. $\text{Mg}^{2+}/\text{Mg}^0$ without any need for pre-removal of any solvent ligand. The open question remaining is the relative concentration of such neutral species at a negatively charged electrode surface, which we do argue should rather favor the above outlined positively charged species. Nonetheless, we have herein identified (at least) two paths by which the plating reactions may occur, by combining the thermodynamic stability data in Table 1 with their reduction potentials and experimental observations: either by a pre-desolvation and subsequent reduction of MgCpTHF_5^+ species, or by a direct reduction of $\text{MgCp}_2\text{THF}_2$ species.

The other ESW limit is largely determined by the oxidation of the Cp^- anion which is calculated to occur at 1.86 V vs. $\text{Mg}^{2+}/\text{Mg}^0$ (Table 1) and matches very well with experimental electrochemical data.^[14] The anodic decomposition of the Cp^- anion basically means the removal of one ring electron and that the aromatic character is lost. Furthermore, the created reactive radical may undergo dimerization producing bis(1,3-cyclopentadiene) ($\Delta G = -154 \text{ kJ mol}^{-1}$, Figure 7). The amount of double bonds in this product may result in further stabilization and a transformation towards naphthalene and cyclopentadiene^[35] is connected with only a very small decrease in energy. In contrast a Diels-Alder reaction can be anticipated; while internal cycloaddition, between two rings of the same

Table 3. DFT calculated Mg plating reactions and associated reduction potentials.

Mg plating reactions	E_{red} [V vs. $\text{Mg}^{2+}/\text{Mg}^0$]
$\text{MgCpTHF}_5^+ + \text{MgCp}_2\text{THF}_2 + 2e^- \rightarrow \text{Mg(s)} + \text{MgCp}_3\text{THF}^- + 6 \text{ THF}$	-0.26
$3 \text{ MgCp}_2\text{THF}_2 + 2e^- \rightarrow \text{Mg(s)} + 2 \text{ MgCp}_3\text{THF}^- + 4 \text{ THF}$	0.06
$2 \text{ MgCpTHF}_5^+ + 2e^- \rightarrow \text{Mg(s)} + \text{MgCp}_2\text{THF}_2 + 8 \text{ THF}$	-0.57
$\text{MgCp}_2 + 2e^- \rightarrow \text{Mg(s)} + 2 \text{ Cp}^-$	0.21
$\text{MgCp}_2\text{THF}_2 + 2e^- \rightarrow \text{Mg(s)} + 2 \text{ Cp}^- + 2 \text{ THF}$	0.22
$\text{MgCpTHF}_5^+ + 2e^- \rightarrow \text{Mg(s)} + \text{Cp}^- + 5 \text{ THF}$	-0.18
$\text{MgCpTHF}_4^+ + 2e^- \rightarrow \text{Mg(s)} + \text{Cp}^- + 4 \text{ THF}$	-0.05
$\text{MgCpTHF}_3^+ + 2e^- \rightarrow \text{Mg(s)} + \text{Cp}^- + 3 \text{ THF}$	0.50

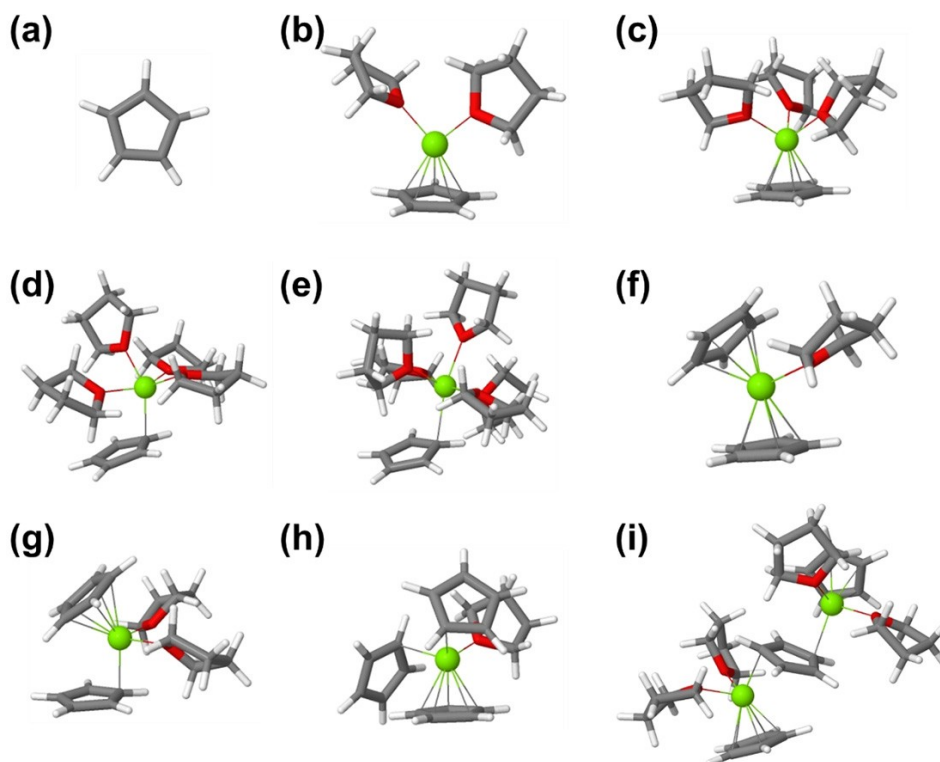


Figure 6. DFT calculated $\text{Mg}_x\text{Cp}_y\text{THF}_z$ structures: a) Cp^- , b) MgCpTHF_2^+ , c) MgCpTHF_3^+ , d) MgCpTHF_4^+ , e) MgCpTHF_5^+ , f) MgCp_2THF , g) $\text{MgCp}_2\text{THF}_2$, h) MgCp_3THF , and i) $\text{Mg}_2\text{Cp}_3\text{THF}_4^+$. Color coding; Mg: green, C: grey, H: white, O: red.

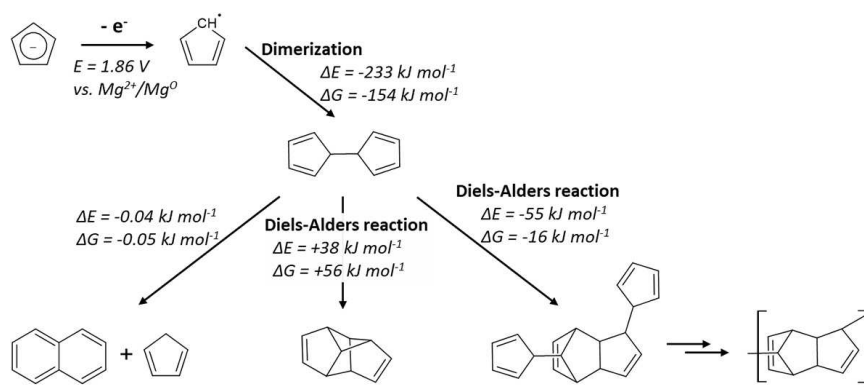


Figure 7. DFT calculated reaction paths for the oxidation and dimerization of the Cp^- anion.

molecule, would result in a structure with huge strain ($\Delta G = +56 \text{ kJ mol}^{-1}$), a reaction between two molecules is exothermal ($\Delta G = -16 \text{ kJ mol}^{-1}$) (Figure 7). As an overall outcome, the Cp^- anion anodic decomposition final product may ultimately be a polymeric structure coating the positive electrode.

2.3. In Silico Cp-Ring Substitutions

From the above it is clear that the Cp^- anion anodic stability is a severely limiting factor for the MgCp_2 in THF electrolyte. Therefore, Cp-ring substitutions, and especially the introduction of electron withdrawing groups, was explored *in silico*, in order

to guide future synthesis efforts towards similar electrolytes with improved ESWs. Four different halogens/pseudohalogens were explored as substituents: $-\text{CN}$, $-\text{F}$, $-\text{Cl}$ and $-\text{Br}$, and indeed some impressive shifts, even up to 4.63 V vs. $\text{Mg}^{2+}/\text{Mg}^0$, were obtained (Table 4). For the most extreme case, $\text{C}_5(\text{CN})_5^-$, this is a combined effect of resonance between the aromatic ring and the triple bonds within $-\text{CN}$ and stabilizing the π electrons, whereas for the halogens only an induction effect is observed and less remarkable, but still significant improvements in the stability: 2.31–2.78 V vs. $\text{Mg}^{2+}/\text{Mg}^0$. The altered electron density also modifies the interaction with the Mg^{2+} cation and this follows the trend of the oxidation stability: $\text{C}_5(\text{CN})_5^- < \text{C}_5\text{Br}_5^- < \text{C}_5\text{Cl}_5^- < \text{C}_5\text{F}_5^-$, all much reduced as com-

Anion	E_{ox} [V vs. Mg^{2+}/Mg^0]	$E_{int Mg^{2+}}$ [$kJ mol^{-1}$]
$Cp^- (C_5H_5^-)$	1.84	319
$C_5F_5^-$	2.31	199
$C_5Cl_5^-$	2.70	178
$C_5Br_5^-$	2.78	175
$C_5(CN)_5^-$	4.63	149

Cluster	$E_{formation}$ [$kJ mol^{-1}$]
$[Mg(C_5H_5)THF_5]^+$	-686
$[Mg(C_5F_5)THF_5]^+$	-679
$[Mg(C_5Cl_5)THF_5]^+$	-674
$[Mg(C_5Br_5)THF_5]^+$	-660
$[Mg[C_5(CN)_5]THF_5]^+$	-651

pared to the Cp^- anion *i.e.* $C_5H_5^-$ (Table 4). Notably, $C_5(CN)_5^-$ was explored *in silico* as an anion for Li-salts and LIB electro-

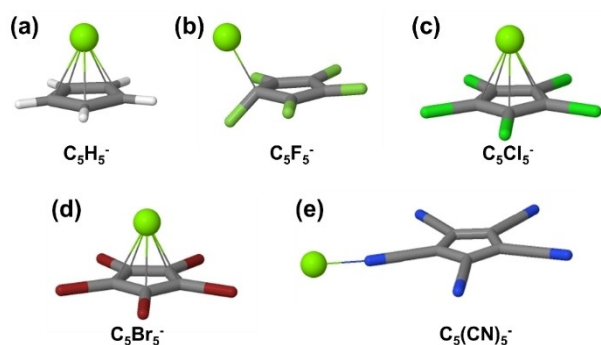


Figure 8. DFT calculated geometries of Mg^{2+} -anion ion-pairs. Color coding; Mg: green, C: grey, H: white, F: lime, Cl: green, Br: maroon, N: blue.

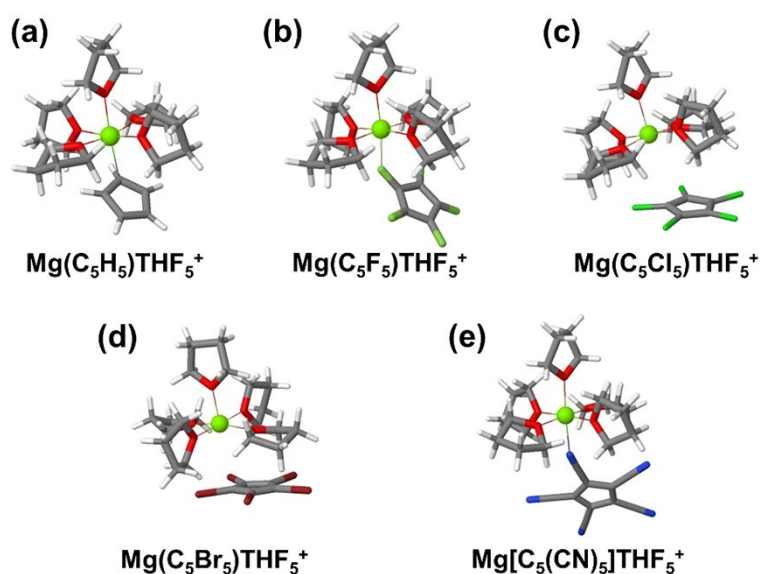


Figure 9. DFT calculated geometries of Mg^{2+} -anion-THF₅ clusters. Color coding; Mg: green, C: grey, H: white, O: red, F: lime, Cl: green, Br: maroon, N: blue.

lytes already in 2004,^[36] as part of a study of systematic -CN substitutions for various Hückel based anions.^[37]

The cation-anion interaction calculations, by means of ion-pairs, were designed to consider both the electron density of the ring and the substituents as interaction sites for the Mg^{2+} cation. For $C_5Br_5^-$ and $C_5Cl_5^-$, as is this case for the Cp^- anion, the former was found to be preferred, while for $C_5F_5^-$ the electron density of the ring is strongly reduced, which renders a site where the Mg^{2+} cation bidentately coordinates a single carbon atom and a fluorine atom the more preferred and furthermore the ring aromaticity seems lost (Figure 8). The even stronger electron withdrawing power of -CN in $C_5(CN)_5^-$ results in a complete preference for substituent coordination by Mg^{2+} , precluding any interaction with the aromatic ring, in agreement with the case for Li^+ as the cation,^[36] which also explains the much weaker interaction overall (Table 4). To make a first crude assessment of whether the above effects also remain within THF-based electrolytes Mg^{2+} -anion-THF₅ clusters were studied and indeed the overall type of coordination from the ion-pairs was retained (Figure 9). With the very similar formation energies for all different anions/substitutions (Table 5) and following the line of argument with respect to the role of solvation for $MgCp_2THF_5^+$ and $MgCp_2THF_2$ above render primarily $C_5Br_5^-$ and $C_5Cl_5^-$ the more interesting Cp^- analogues.

3. Conclusions

The combination of $MgCp_2$ salt dissolved in THF renders an electrolyte with a very good cathodic stability and high Mg stripping/plating efficiency over many cycles, which paves the way for low voltage Mg battery cells. The stability of this Mg battery chemistry is further supported by XPS analysis of the electroplated Mg, which does not reveal any major electrolyte decomposition products or surface passivation layers. Combin-

ing experimental data with DFT calculations we find that anodically the electrolyte is stable up to ca. 1.5–1.8 V vs. $\text{Mg}^{2+}/\text{Mg}^{\circ}$ and this is ultimately limited by the stability of the Cp^{-} anion that is oxidized to the neutral radical Cp^{\bullet} , followed by dimerization and most likely also subsequent Diels-Alder reactions. Within the electrolyte $\text{MgCp}_2\text{THF}_2$ is the most stable neutral species, wherein one Cp moiety is η^5 -coordinated and the other η^1 -coordinated, and the two THF solvent molecules are coordinated via their oxygen atoms. Thus the structure previously resolved for solid $\text{MgCp}_2\text{THF}_2$ ^[21] is preserved in solution. As the cathodic stability of $\text{MgCp}_2\text{THF}_2$ is well below 0 V vs. $\text{Mg}^{2+}/\text{Mg}^{\circ}$ this species is most likely not the species reduced during Mg stripping/plating reactions and the very absence of any decomposition is a huge advantage of these magnesocene based electrolytes, as any passivation film is believed to completely preclude Mg battery operation. Tailored *in silico* substitutions allow us to predict some much more electrochemically stable and more weakly interacting Cp^{-} anion derivatives and taking into account the experimental as well as computational knowledge gained on the role of MgCp_2 solvation by THF, we suggest primarily $\text{C}_5\text{Br}_5^{-}$ and $\text{C}_5\text{Cl}_5^{-}$ to be viable Cp^{-} analogues to explore further.

Acknowledgements

The authors would like to thank Claudia Pfeifer (ZSW) for recording the SEM image. P.J. and P.J. acknowledge the support from Honda R&D Europe and several of Chalmers Areas of Advance: Materials Science, Energy and Transport. R.S. and M.W. acknowledge the financial support from the German Federal Ministry of Education and Research (BMBF) (project "Mg-Air", 03EK3027C). R.Y. and M.W. acknowledges the support from the Swedish Government (Swedish Strategic Research Programme "STandUP for Energy"). All DFT calculations were carried out at the Wrocław Centre for Networking and Supercomputing, Grant 346.

Conflict of Interest

The authors declare no conflict of interest.

Keywords: bis(cyclopentadienyl) magnesium · density functional theory · electrochemical stability window · electrolyte decomposition reactions · magnesium electroplating

- Huang, Z. Zhou, P. Johansson, M. Forsyth, *Angew. Chem. Int. Ed.* **2019**, *58*, 2–7; *Angew. Chem.* **2019**, *131*, 2–2.
- [2] A. Ponrouch, J. Bitenc, R. Dominko, N. Lindahl, P. Johansson, M. R. Palacin, *Energy Storage Mater.* **2019**, *20*, 253–262.
- [3] D. Aurbach, Z. Lu, Z. A. Schechter, Y. Gofer, H. Gizbar, R. Turgeman, Y. Cohen, M. Moshkovich, E. Levi, *Nature* **2000**, *407*, 724–727.
- [4] R. D. Shannon, C. T. Prewitt, *Acta Crystallogr.* **1969**, *B25*, 925–946.
- [5] N. N. Greenwood, E. A. Earnshaw, *Chemistry of the Elements*. (1984) Oxford, UK: Pergamon Press.
- [6] U. S. Geological Survey (2018). *Mineral Commodity Summaries*.
- [7] M. Matsui, *J. Power Sources* **2011**, *196*, 7048–7055.
- [8] D. Aurbach, Y. Cohen, M. Moshkovich, *Electrochem. Solid-State Lett.* **2001**, *4*, A113–A116.
- [9] J. G. Connell, B. Genorio, P. P. Lopes, D. Strmcnik, V. R. Stamenkovic, N. M. Markovic, *Chem. Mater.* **2016**, *28*, 8268–8277.
- [10] D. Tchitchekova, D. Monti, P. Johansson, F. Bardé, A. Randon-Vitanova, M. R. Palacin, A. Ponrouch, *J. Electrochem. Soc.* **2017**, *164*, A1384–A1392.
- [11] C. Liao, N. Sa, B. Key, A. K. Burrell, L. Cheng, L. A. Curtiss, J. T. Vaughey, J.-J. Woo, L. Hu, B. Pan, Z. Zhang, *J. Mater. Chem. A* **2015**, *3*, 6082–6087.
- [12] Z. Zhao-Karger, M. E. Gil Bardaji, O. Fuhr, M. Fichtner, *J. Mater. Chem. A* **2017**, *5*, 10815–10820.
- [13] A. L. Lipson, S.-D. Han, B. Pan, K. A. See, A. A. Gewirth, C. Liao, J. T. Vaughey, B. J. Ingram, *J. Electrochem. Soc.* **2016**, *163*, A2253–A2257.
- [14] R. Schwarz, M. Pejic, P. Fischer, M. Marinaro, L. Jörissen, M. Wachtler, *Angew. Chem. Int. Ed.* **2016**, *55*, 14958–14962; *Angew. Chem.* **2016**, *128*, 15182–15186.
- [15] W. Bünder, E. Weiss, *J. Organomet. Chem.* **1975**, *92*, 1–6.
- [16] W. Strohmeier, H. Landsfeld, F. Gernert, *Z. Elektrochem.* **1962**, *66*, 823–827.
- [17] W. Strohmeier, F. Seifert, H. Landsfeld, *Z. Elektrochem.* **1962**, *66*, 312–316.
- [18] R. M. Fuoss, C. A. Kraus, *J. Am. Chem. Soc.* **1933**, *55*, 476–488.
- [19] R. M. Fuoss, C. A. Kraus, *J. Am. Chem. Soc.* **1933**, *55*, 2387–2399.
- [20] A. Haaland, J. Lusztyk, J. Brunvoll, K. B. Starowieyski, *J. Organomet. Chem.* **1975**, *85*, 279–285.
- [21] E. Weiss, E. O. Fischer, *Z. Anorg. Allg. Chem.* **1955**, *278*, 219–224.
- [22] A. Jaenschke, J. Paap, U. Behrens, *Z. Anorg. Allg. Chem.* **2008**, *634*, 461–469.
- [23] H. Lehmkuhl, K. Mehler, R. Benn, A. Ruffińska, C. Krüger, *Chem. Ber.* **1986**, *119*, 1054–1069.
- [24] A. Jaenschke, J. Paap, U. Behrens, *Organometallics* **2003**, *22*, 1167–1169.
- [25] K. M. Abraham, J. L. Goldman, *J. Power Sources* **1983**, *9*, 239–245.
- [26] K. Xu, *Chem. Rev.* **2004**, *104*, 4303–4417.
- [27] M. J. Frisch, G. W. Trucks, H. B. Schlegel, *Gaussian 16, Revision B.01*. (2016). Gaussian Inc., Wallingford, CT.
- [28] Y. Zhao, D. G. Truhlar, *Theor. Chem. Acc.* **2008**, *120*, 215–241.
- [29] E. Cancès, B. Mennucci, J. Tomasi, *J. Chem. Phys.* **1997**, *107*, 3032–3041.
- [30] P. Jankowski, W. Wiczeorek, P. Johansson, *J. Mol. Model.* **2017**, *23*, 6.
- [31] A. E. Reed, R. B. Weinstock, F. Weinhold, *J. Chem. Phys.* **1985**, *83*, 735.
- [32] Y. Gofer, R. Turgeman, H. Cohen, D. Aurbach, *Langmuir* **2003**, *19*, 2344–2348.
- [33] O. Tutusaus, R. Mohtadi, N. Singh, T. S. Arthur, F. Mizuno, *ACS Energy Lett.* **2017**, *2*, 224–229.
- [34] P. Jankowski, J. M. García Lastra, T. Vegge, *Batteries & Supercaps* **2020**, *3*, 1350–1359; *Supercaps* **2020**, *3*, 1350–1359.
- [35] V. V. Kislov, A. M. Mebel, *J. Phys. Chem. A* **2007**, *111*, 9532–9543.
- [36] P. Johansson, H. Markusson, P. Jacobsson, M. Armand, *Phys. Chem. Chem. Phys.* **2004**, *6*, 895–899.
- [37] M. Armand, P. Johansson, M. Bukowska, P. Szczeciński, L. Niedzicki, M. Marcinek, M. Dranka, J. Zachara, G. Żukowska, M. Marczewski, G. Schmidt, W. Wiczeorek, *J. Electrochem. Soc.* **2020**, *167*, 070562.

Manuscript received: February 5, 2021

Revised manuscript received: March 25, 2021

Accepted manuscript online: April 7, 2021

Version of record online: May 5, 2021

[1] H. Zhang, C. Li, G. G. Eshetu, S. Laruelle, S. Grugeon, K. Zaghib, C. Julien, A. Mauger, D. Guyomard, T. Rojo, N. Gisbert-Trejo, S. Passerini, X.